

Technical Paper:

# Vibration Mode and Motion Trajectory Simulations of an Articulated Robot by a Dynamic Model Considering Joint Bearing Stiffness

Ryuta Sato<sup>\*,†</sup>, Yuya Ito<sup>\*\*</sup>, Shigeto Mizuura<sup>\*\*</sup>, and Keiichi Shirase<sup>\*</sup>

<sup>\*</sup>Department of Mechanical Engineering, Kobe University  
1-1 Rokko-dai, Nada-ku, Kobe 657-8501, Japan

<sup>†</sup>Corresponding author, E-mail: sato@mech.kobe-u.ac.jp

<sup>\*\*</sup>DAIHEN Corporation, Kobe, Japan

[Received March 24, 2021; accepted May 18, 2021]

Articulated robots are widely used in industries because they can perform manufacturing tasks with complicated movements. Higher speed and accuracy of motions are always required to improve the quality and productivity of products. The vibration characteristics of the robots are an important factor to achieve higher speed and accuracy motions. Robots are increasingly being used for machining. The vibration characteristics must also be considered when designing proper cutting conditions for the machining. To design control and cutting strategies for higher speed and accuracy motions or higher productivity of the machining process, it is effective to investigate the vibration characteristics of the robot and develop a mathematical model which can represent the vibration characteristics. The aim of this study is to investigate the vibration characteristics of an architectural robot and develop a mathematical model which can represent the dynamic behavior of the robot. To achieve this, vibration mode of an industrial architectural robot is analyzed based on measured frequency characteristics. According to the results of the modal analysis, it was clarified that the axial and angular stiffness of bearings of each joint of the robot has a significant impact on the vibration characteristics. Therefore, in this study, a mathematical model of the robot is developed considering the joint bearing stiffness. The mathematical model that also considers the kinematics of the robot, stiffness of reduction gears, control system for motors, and disturbance, such as friction and gravity, is introduced into the model. The control system is precisely modeled based on actual control algorithm in accordance with the implemented source codes. Although mass and inertia of the links are obtained from the 3D-CAD model, stiffness and damping parameters of the bearings and reduction gears are identified by matching the measured and simulated frequency responses. It has been confirmed that the model can adequately represent the vibration mode of the actual robot. Circular motion tests were performed to verify the model. Motion trajectories of the end effector were measured and simulated. As a

result, it has been confirmed that the developed model is effective to analyze the dynamic behaviors.

**Keywords:** articulated robot, mathematical model, joint bearing stiffness, vibration mode, circular trajectory

## 1. Introduction

Articulated robots are widely used in industries, particularly in the fields of welding, material handling, and painting [1]. The motion accuracy of an industrial robot is important because it is directly linked to the quality and productivity of products. However, owing to the low mechanical stiffness of the robot, extreme overshoot and vibration tend to occur when the robot moves at high speed. To achieve faster and more accurate robot motion, the robot motion should be analyzed using a model capable of expressing dynamic behaviors [2]. In addition, machining operations are becoming another application of robots [3]. Many researchers have attempted to apply robots to machining operations [4–8]. The vibration characteristics of the robot play a key role in achieving higher productivity, and it is necessary to predict the vibration characteristics because the relationship between the cutting condition and vibration characteristics determines the chatter stability [9, 10].

Articulated robots can be modeled by considering the link kinematics, inertial parameters of the links, characteristics of driving mechanisms, and control systems [11]. Zirn [12] described a general approach to model the manipulators represented as state equations. Several studies have also been conducted on robot arm modeling [13–19]. They mainly focused on kinematical modeling problems. Good et al. [20] focused on the influence of the stiffness of the reduction gears and friction. However, the influence of stiffness on the dynamic behavior has not been investigated. It is necessary to clarify and predict the dynamic behavior of robots to expand their applications [21, 22].

The aim of this study is to investigate the vibration characteristics of an architectural robot and develop a



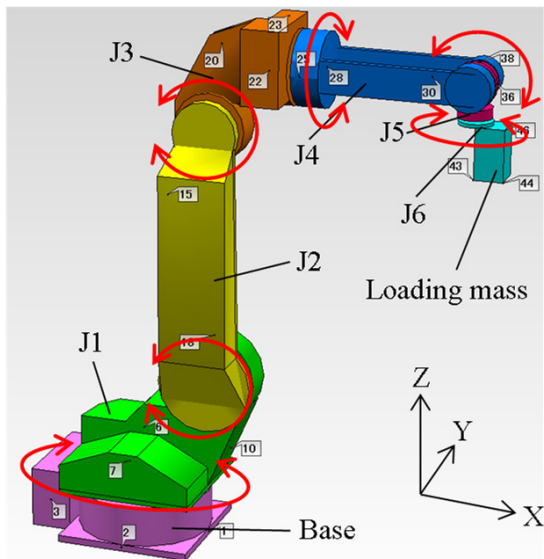


Fig. 1. Architectural robot and measurement points.

mathematical model that can represent its dynamic behavior. To achieve this, the vibration mode of an industrial architectural robot was analyzed based on measured frequency characteristics. According to the results of the modal analysis, it was clarified that the axial and angular stiffness of the bearings of each joint of the robot has a significant impact on the vibration characteristics. Bottin et al. [23] also highlighted that the joint bearing stiffness impacts the vibration characteristics of robots. Although the identification method for the stiffness and predicted natural frequencies based on the identified results are presented, the simulated vibration mode and motion trajectories are not discussed.

Therefore, in this study, a mathematical model of the robot was developed by considering the joint bearing stiffness. The vibration mode and motion trajectories were simulated to demonstrate the effectiveness of the model. The mathematical model that also considers the kinematics of the robot, stiffness of reduction gears, control system for motors, and disturbances, such as friction and gravity, is introduced into the model.

## 2. Modal Analysis

### 2.1. An Arbitrated Robot and Measurement Method

Figure 1 illustrates the articulated robot modeled in this study. The robot has six links, J1–J6. J1–J4 links are driven by AC servo motors and cycloidal reduction gears, and J5 and J6 links are driven by AC servo motors and timing belts. The joint between the links was connected by ball bearings.

A loading mass assuming the welding touch or milling spindle was attached to the J6 link to express the real situations in the field. Another loading mass is also attached

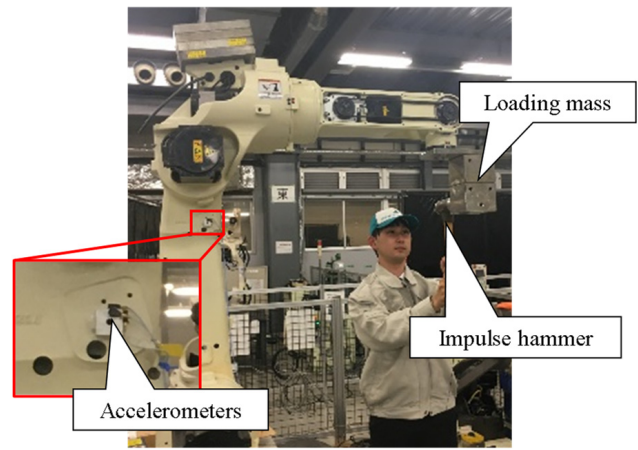


Fig. 2. Hammering test.

to the J3 link, assuming the controller and drivers for the equipment attached to link J6.

The loading mass attached to link J6 was excited by an impulse hammer, as shown in Fig. 2. Three directional accelerations at a total of 48 points on the base and J1–J6 links were measured. The accelerometers were attached to the surface through an aluminum cubic block. Hammering tests were conducted by changing the measurement point, and five measurements were taken for each point (a total of 240 hammering). The inductance transfer function between the excitation and measurement points was measured.

It is also known that the condition of servo drive system influences the frequency characteristics [24]. In this study, to evaluate the characteristics under the same real conditions in the field, the measurements were conducted under the servo-on condition. This means that the mechanical brakes of all the servo motors were unclamped, and the motor angles were maintained by the feedback control system during the measurement.

### 2.2. Frequency Characteristics and Vibration Mode

Figure 3 shows the measured frequency responses of each point. The figure only shows the selected data for representative measurement points. It can be observed from the figure that the first vibration mode is around 10 Hz and second is around 20 Hz. It can also be observed that the vibration amplitude becomes largest at the measurement points on the link J6 at the first and second resonance frequencies. In addition, because it has been confirmed that the first vibration mode at approximately 10 Hz is a dominant problem during the motions, the first vibration mode is the primary focus of this study.

Figure 4 illustrates the first vibration mode analyzed from the measured frequency responses. The results show that the dominant vibration comes from the following vibrations: translational vibration between J1 and J2 links along the Y-axis, angular vibration between J1 and J2 links around the X-axis, translational vibration between

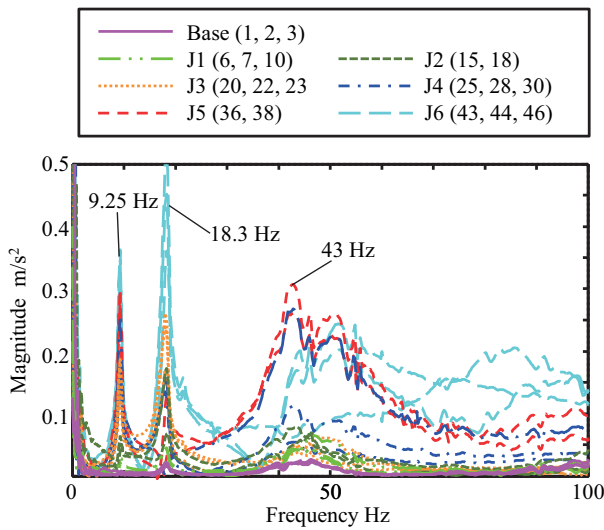


Fig. 3. Measured frequency responses for modal analysis.

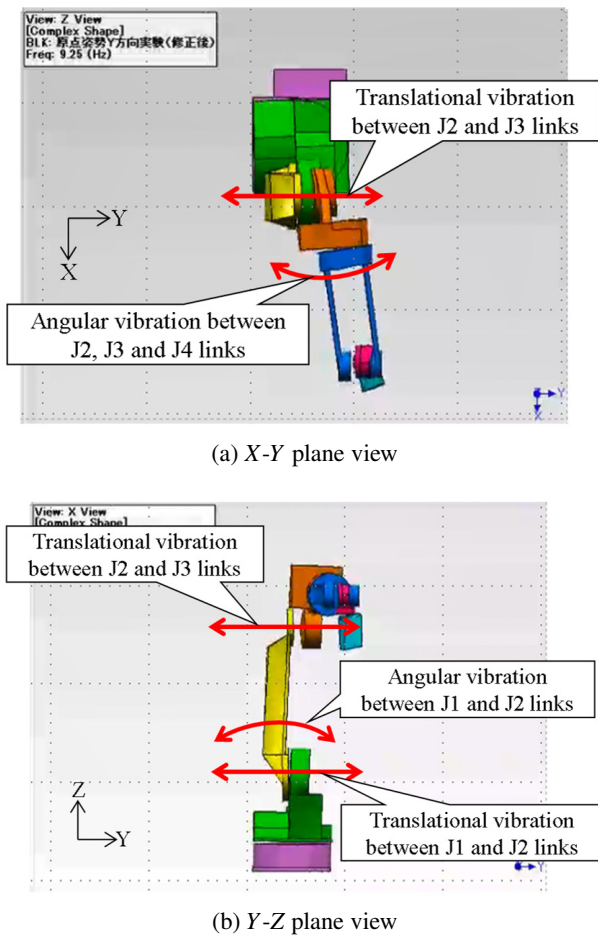


Fig. 4. Analyzed modal shape with Y-axis excitation.

J2 and J3 links along the Y-axis, and angular vibration between the J2, J3, and J4 links. The analyzed results suggest that the axial and angular stiffness of the joint bearings plays a key role in the vibration characteristics of the articulated robot.

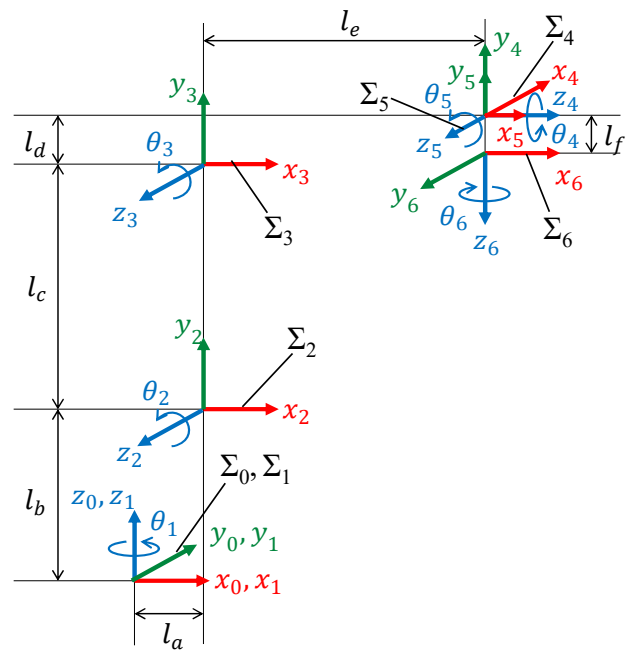


Fig. 5. Coordinate system for D-H matrix.

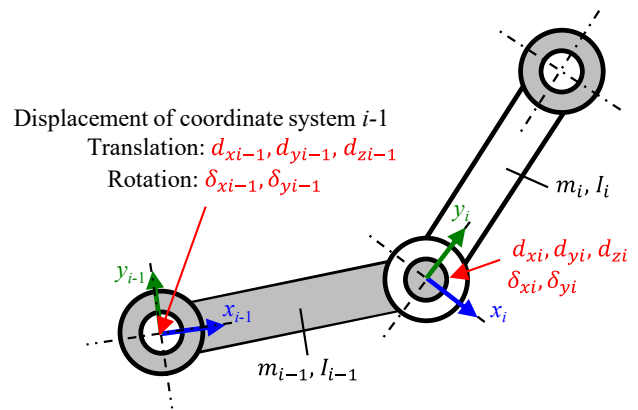


Fig. 6. Definition of translational and angular deformation between links.

### 3. Mathematical Modeling

#### 3.1. Link Model with Joint Bearing Stiffness

The link kinematics of the robot is modeled by the Denavit-Hartenberg (D-H) matrix based on the coordinate systems shown in Fig. 5 [25]. The coordinate system for J1 link  $\Sigma_1$  is identical to the world coordinate system  $\Sigma_0$  in this study. To represent the translational and angular deformation of the bearing between the links, small angular and translational displacements between the links are introduced, as illustrated in Fig. 6. The translational displacement along the X-, Y-, and Z-axes and angular displacement around the X- and Y-axes of each joint are considered. The angular displacement around the Z-axis indicates the rotational angle of the joint. The displacements can be calculated based on the angular, axial, and radial stiffness of the joint bearings, and the acting forces

and torques on the bearings are calculated based on the equation of motion.

Equation of motion of a robot can be represented as follows:

$$M\ddot{q} + c\dot{q} + kq = Q \dots \dots \dots (1)$$

It can be rewritten as Eq. (2) by substituting Eq. (3).

$$M_{(q)}\ddot{q} + H_{(q,\dot{q})} = Q \dots \dots \dots (2)$$

$$H = c\dot{q} + kq \dots \dots \dots (3)$$

where  $M$  is a  $36 \times 36$  matrix that represents the mass and inertia of each link. This depends on the angle of each joint. Matrices  $c$  and  $k$  are also  $36 \times 36$  matrices that represent the damping and stiffness between the links by considering the relative displacement and velocity of the links as non-diagonal elements. The stiffness matrix  $k$  includes the influence of gravity, and it also depends on the angle of each joint. Note that the angular stiffness and damping around the Z-axis of each link are not considered in the equation of motion. This will be introduced into the model of the driving mechanism.

As a result,  $H$  is a  $36 \times 1$  vector that represents the influence of gravity, Coriolis and centrifugal forces, and mutual interference of links. It also depends on the angle and angular velocity of each joint. It is assumed that the relative displacements owing to the elastic deformation of the joint bearings are small and their influence can be linearly approximated. Because it was difficult to obtain each element of the matrices, a commercial software Maple (MathWorks, Inc.) was applied to solve the equations.

The model in this study has 36 degrees of freedom (DOF) because each link has six DOFs.  $q$  is the  $36 \times 1$  vector that represents the relative displacements and angles between the links, and  $Q$  is the  $36 \times 1$  vector that represents the external forces or torques relative to the links as follows:

$$q = [d_{x1} \ d_{y1} \ d_{z1} \ \delta_{x1} \ \delta_{y1} \ \theta_1 \ d_{x2} \ d_{y2} \ d_{z2} \ \delta_{x2} \ \delta_{y2} \ \theta_2 \ \dots \ d_{x6} \ d_{y6} \ d_{z6} \ \delta_{x6} \ \delta_{y6} \ \theta_6]^T \quad (4)$$

$$Q = [0 \ 0 \ 0 \ 0 \ 0 \ \tau_1 \ 0 \ 0 \ 0 \ 0 \ 0 \ \tau_2 \ \dots \ 0 \ 0 \ 0 \ 0 \ 0 \ \tau_6]^T \quad (5)$$

where  $\tau_1$ – $\tau_6$  represent the driving torques applied from the driving mechanisms of each link. The excitation force generated by the impulse hammer can be considered as a component of  $Q$  in the simulation. Disturbance forces, such as cutting forces, can also be considered in  $Q$ .

The kinetic energy,  $T$ , potential energy,  $U$ , and dissipated energy,  $F$ , of the robot can be expressed as follows:

$$T = \frac{1}{2} \sum m_i \dot{x}_{Gi}^2 + \frac{1}{2} \sum m_i \dot{y}_{Gi}^2 + \frac{1}{2} \sum m_i \dot{z}_{Gi}^2 + \frac{1}{2} \sum \omega_i^T I_i \omega_i \dots \dots \dots (6)$$

$$U = \sum m_i g z_{Gi} + \frac{1}{2} \sum K_{xi} d_{xi}^2 + \frac{1}{2} \sum K_{yi} d_{yi}^2 + \frac{1}{2} \sum K_{zi} d_{zi}^2 + \frac{1}{2} \sum K_{\delta_{xi}} \delta_{xi}^2 + \frac{1}{2} \sum K_{\delta_{yi}} \delta_{yi}^2 \quad (7)$$

$$F = \frac{1}{2} \sum c_{xi} d_{xi}^2 + \frac{1}{2} \sum c_{yi} d_{yi}^2 + \frac{1}{2} \sum c_{zi} d_{zi}^2 + \frac{1}{2} \sum c_{\delta_{xi}} \delta_{xi}^2 + \frac{1}{2} \sum c_{\delta_{yi}} \delta_{yi}^2 \dots \dots \dots (8)$$

where the subscript  $i$  represents the number of links ( $i = 1$ – $6$ ). The kinetic energy  $T$  can be defined from the velocity of the center of gravity of each link  $\dot{x}_{Gi}$ ,  $\dot{y}_{Gi}$ ,  $\dot{z}_{Gi}$  and the angular velocity of each link  $\omega_i$ . These parameters can be obtained based on the D-H matrix. The potential energy,  $U$ , can also be defined from the radial deformations and stiffness of each joint bearing,  $d_{xi}$ ,  $d_{yi}$  and  $K_{xi}$ ,  $K_{yi}$ , axial deformations and stiffness of the joint bearings,  $d_{zi}$  and  $K_{zi}$ , angular deformations and stiffness around the X- and Y-axes of the joint bearings,  $\delta_{xi}$ ,  $\delta_{yi}$  and  $K_{\delta_{xi}}$ ,  $K_{\delta_{yi}}$ . The influence of gravity is also considered as a part of the potential energy based on the Z-axis position of each link,  $z_{Gi}$ . The dissipated energy,  $F$ , can similarly be defined based on the radial and axial viscose coefficients  $c_{xi}$ ,  $c_{yi}$ , and  $c_{zi}$ , and angular viscose coefficients  $c_{\delta_{xi}}$  and  $c_{\delta_{yi}}$ . The angular stiffness and viscose coefficient around the Z-axis were modeled as a part of the driving mechanisms. The equation of motion can be obtained by solving the Lagrange method based on the defined energies  $T$ ,  $U$ , and  $F$ .

Equation (2) can be deformed as follows:

$$\ddot{q} = M_{(q)}^{-1} (Q - H_{(q,\dot{q})}) \dots \dots \dots (9)$$

As a result, the articulated robot model can be represented by a block diagram, as shown in **Fig. 7**. Matrix  $M$  and vector  $H$  are functions of the model output vector  $q$ . All simulations in this study were conducted using MATLAB Simulink (MathWorks, Inc.). The parameters  $M$  and  $H$  were updated for each calculation step during the simulation. The matrices obtained by Maple software can be directly transformed into the MATLAB script. As aforementioned, the model shown in **Fig. 7** lacks rotational stiffness and damping around the rotational direction of the bearings. It behaves just like a robot without a driving mechanism with free rotation of the links.

### 3.2. Drive Mechanism

The drive mechanisms of each link were modeled as illustrated in **Fig. 8**, where  $\theta_{mi}$  and  $\tau_i$  represent the rotational angle and driving torque of the motor, respectively. The driving torque was simulated using a controller model.  $K_\theta$  and  $c_\theta$  represent the angular stiffness and damping of the driving mechanism, respectively. The torque applied to the links was generated from the relative angle between the links and motor in this model, where  $n$  is the reduction ratio.

The moment of inertia of the motor rotor  $J_m$  is a known parameter from the specification sheet. However, friction characteristics, modeled in this study as Coulomb's friction torque  $f_m$  and viscose friction coefficient  $D_m$ , must be identified from the measured results. Therefore, the friction parameters for each motor were identified based on the acquired motor torques during the sinusoidal motions

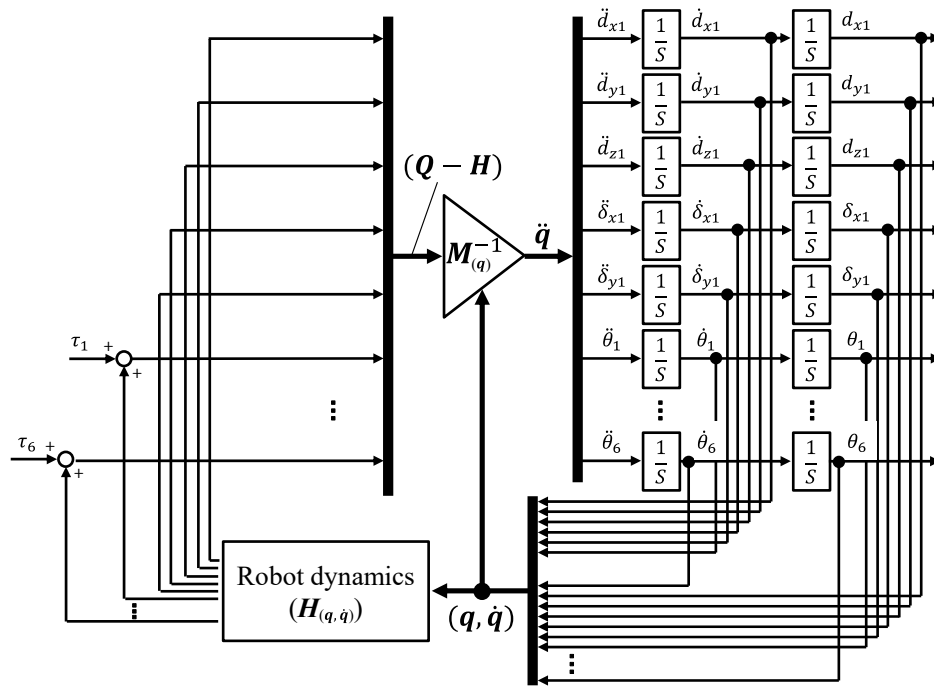


Fig. 7. Block diagram of the proposed robot model with joint bearing stiffness.

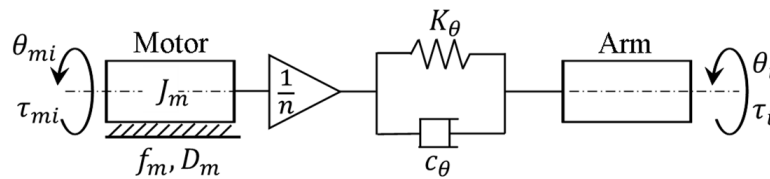


Fig. 8. Schematics of vibration model for driving mechanism.

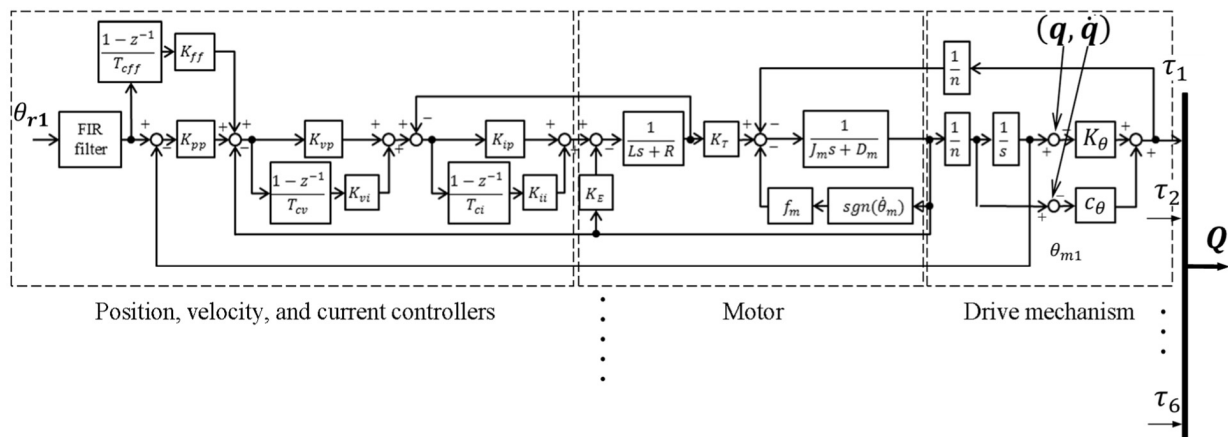


Fig. 9. Block diagram of controller, motor, and drive mechanism.

of each axis [26]. This indicates that the identified friction parameters include both the friction of the motor bearing and joint bearing.

### 3.3. Control System

The control systems of each motor are modeled based on the specifications and source code of the real imple-

mented controllers. Fig. 9 shows the block diagram of the controller, motor, and drive mechanism of an axis. The controller consists of a velocity feed forward controller, position controller, velocity controller, and current controller. Each controller was modeled as a discrete-time system with different control periods. All servo gains and filter parameters were known and used for the simulations

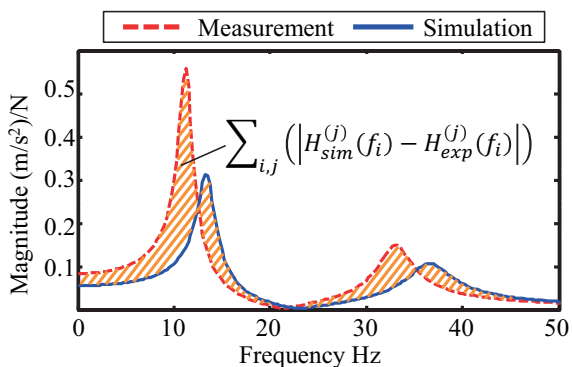


**Fig. 10.** Schematics of parameter identification strategy by using genetic algorithm (GA).

in this study. In addition, the angular command for the motors was acquired from the controller during the experiments, and the acquired data were used for the simulations.

### 4. Parameter Identification

#### 4.1. Identification Method

In this study, the mass and moment of inertia of the links were accurately calculated using the 3D-CAD model of each link. However, it is impossible or difficult to obtain accurate values of the joint bearing stiffness and damping. It is also difficult to calculate the stiffness and damping of the drive mechanisms. Therefore, the stiffness and damping parameters are identified by matching the measured and simulated frequency responses.

A total of 72 parameters were identified. To identify the parameters, a genetic algorithm (GA) [27] that can minimize the fitness function  $F$  defined in Eq. (10) is applied.

$$F = \sum_{i,j} (|H_{sim}^{(j)}(f_i) - H_{exp}^{(j)}(f_i)|) \dots \dots (10)$$

where  $H_{sim}^{(j)}$  and  $H_{exp}^{(j)}$  represent the simulated and measured frequency responses at the measurement point  $j$ , respectively.  $f_i$  represents the frequency. The fitness function  $F$  indicates the total area of the difference between the measured and simulated results, as illustrated in **Fig. 10**. To reduce the load of calculations, two measurement points for each link (12 points in total) were selected and applied for identification.

However, it was difficult to certify the convergence of the solution when attempting to identify all of the parameters simultaneously. Therefore, in this study, first the parameters for the J1–J3 links were identified. This means that the J4–J6 links were detached from the robot, as shown in **Fig. 11**, and frequency responses were measured using hammering tests, as mentioned in Section 2. The J3 link oscillated along the  $Y$ -axis direction in the tests, as shown in **Fig. 11**. Subsequently, the parameters for the J4–J6 links were identified based on the measured frequency responses with the entire robot configuration.

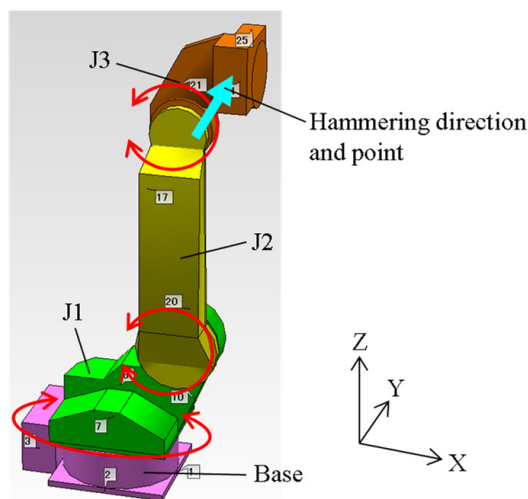


**Fig. 11.** Architectural robot and measurement points without J4–J6 links.

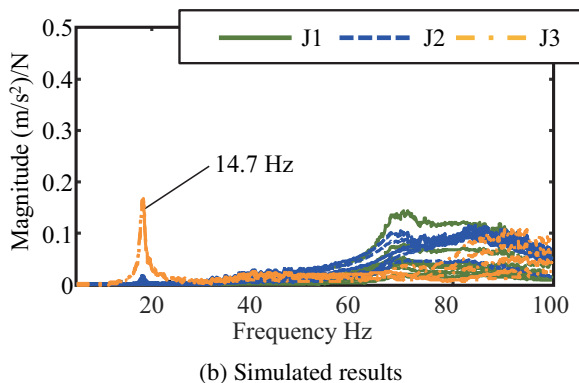
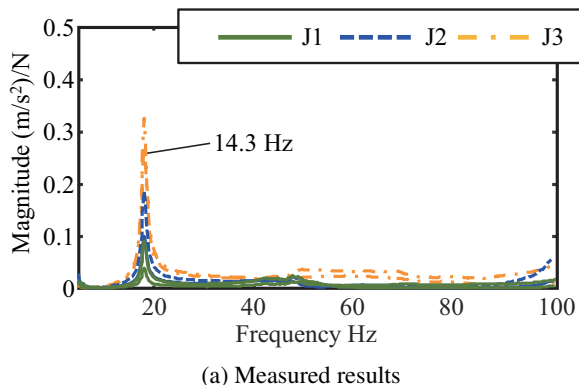


**Fig. 12.** Comparison of measured and simulated frequency responses of J1–J3 links.

#### 4.2. J1–J3 Links

**Figure 12(a)** shows the measured frequency responses without J4–J6 links. The measured frequency response appears to be much simpler than the response of the entire robot configuration, as shown in **Fig. 3**. The resonance frequency was approximately 15 Hz, and it was the translational and rotational vibrations between the J1 and J2 links. This corresponds to a vibration at approximately 10 Hz, as shown in **Fig. 3**.

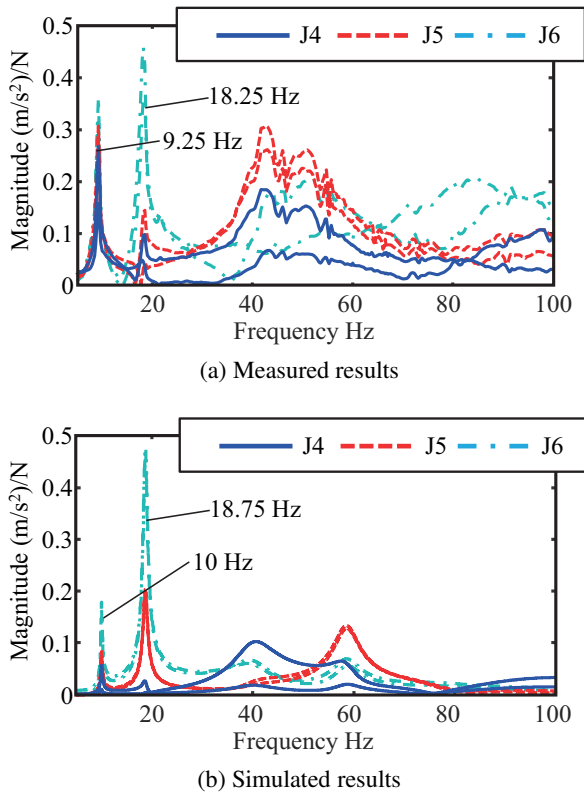


**Fig. 13.** Comparison of measured and simulated frequency responses of J4–J6 links.

The simulated frequency responses based on the identified parameters are shown in **Fig. 12(b)**. According to the results, the amplitude of the vibration is considerably smaller than the measured ones, although the resonance frequency is adequately expressed. It is expected that the reason for the differences is that the base and J1 link have elastic deformation in a real situation. All the components were modeled as rigid in the model. It is necessary to add an additional coordinate transformation between the world and  $\Sigma_1$  coordinate systems to achieve more accurate simulation results.

### 4.3. J4–J6 Links

**Figure 13** shows measured and simulated frequency responses of J4–J6 links with entire robot configuration. It can be observed from the results that the proposed model can correctly predict the resonance frequency of the first and second vibration mode. The resonance frequency shown in **Fig. 12** is approximately 15 Hz and the vibration mode of the frequency corresponds to the first vibration mode in the frequency response shown in **Fig. 13** at approximately 10 Hz. Because of the influence of the mass and inertial of the moment of J4–J6 links, the resonance frequency becomes smaller in **Fig. 13** than the frequency in **Fig. 12**.

It was also identified that although J1–J3 links and J4–J6 links oscillate in the same phase at the first vibration mode at approximately 10 Hz, the J1–J3 links and J4–J6

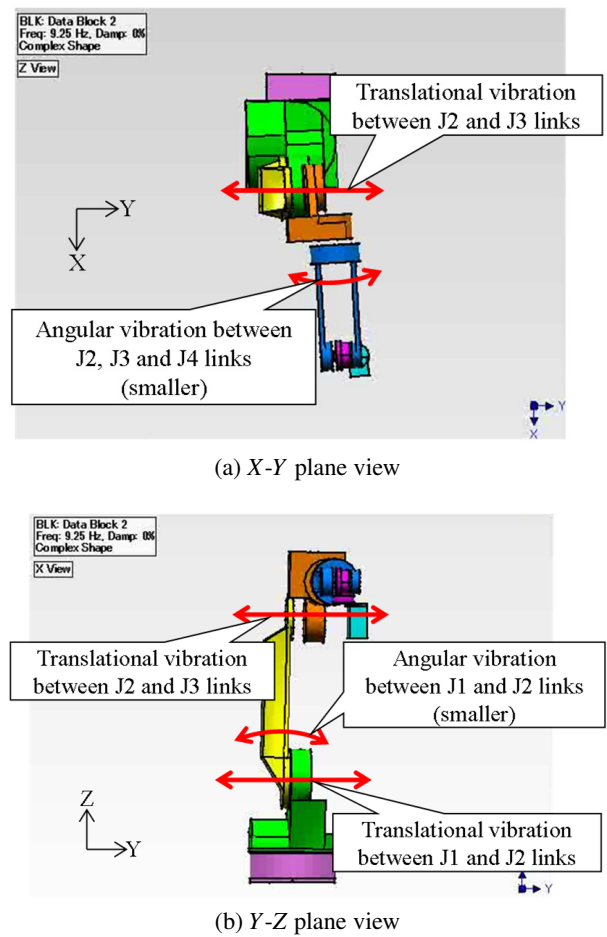


**Fig. 14.** Simulated modal shape with Y-axis excitation.

links oscillate in the opposite phase at the second vibration mode at approximately 20 Hz.

The simulated amplitude of the first vibration mode is smaller than the measured amplitude, similar to the results shown in **Fig. 12**. The reason for the difference can be expected to be as discussed in Section 4.2.

## 5. Comparison of Measured and Simulated Results

### 5.1. Vibration Mode

The modal shape of the first vibration mode is analyzed from the simulated frequency responses, as shown in **Fig. 14**. The results confirm that the proposed model can adequately express the translational and angular vibrations between J1 and J2 links, translational vibration between J2 and J3 links, and angular vibration between J2, J3, and J4 links. However, it was also confirmed that the simulated angular vibrations between the J1, J2 axes, and J2–J4 axes were smaller than the actual ones. In addition, it was confirmed that the proposed model can adequately express the second vibration mode.

Although all the links were modeled as rigid bodies in this study, it is expected that the deformations of each link

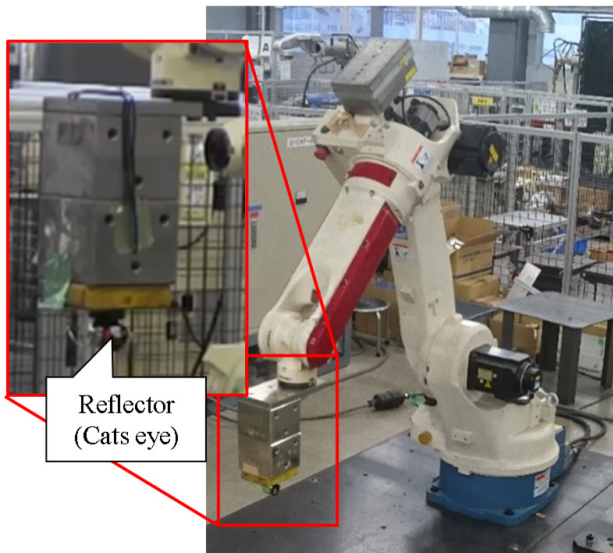


**Fig. 15.** Measurement point and initial posture of the robot for circular motion test.

will affect the angular vibrations. It is also expected that the simulation results can be improved by accurately tuning the identified parameters. However, it can be concluded that the proposed model can adequately express the vibration owing to the joint bearing stiffness, except for the simulation accuracy.

## 5.2. Circular Trajectory

Finally, to evaluate the validity of the model, circular motion tests were conducted. The motion trajectories were measured using a laser tracker (FARO Vantage). A reflector for the measurement was attached to the loading mass, as shown in **Fig. 15**. The robot posture was set to the middle of the working area, as shown in the figure. The model can also represent the influence of the posture.

The feed rate and radius of the circular motion were set to 2000 mm/min and 5 mm, respectively. The robot also has geometric error sources, such as link-length errors. If circular motion with a larger radius is measured, the influence of geometric errors on the trajectory becomes a significant cause of inaccuracy. However, the purpose of this study and the test was to simulate the vibration characteristics of the robot and confirm the correctness of the simulated vibration characteristics. Therefore, a circular trajectory with a smaller radius was measured and simulated. In other words, the results represent only the vibration characteristics at the measurement point.

**Figure 16** shows measured and simulated circular trajectories. The figure represents enlarged radial error from the reference circle. A circle with averaged radius of the trajectory is adopted as the reference circle. This representation is commonly used in machine tool field to evaluate the circular trajectory as a “circular test [28].”

The feedback position means that the calculated trajectory from the acquired rotational angle of the motors is based on the kinematic model. Tracking errors observed

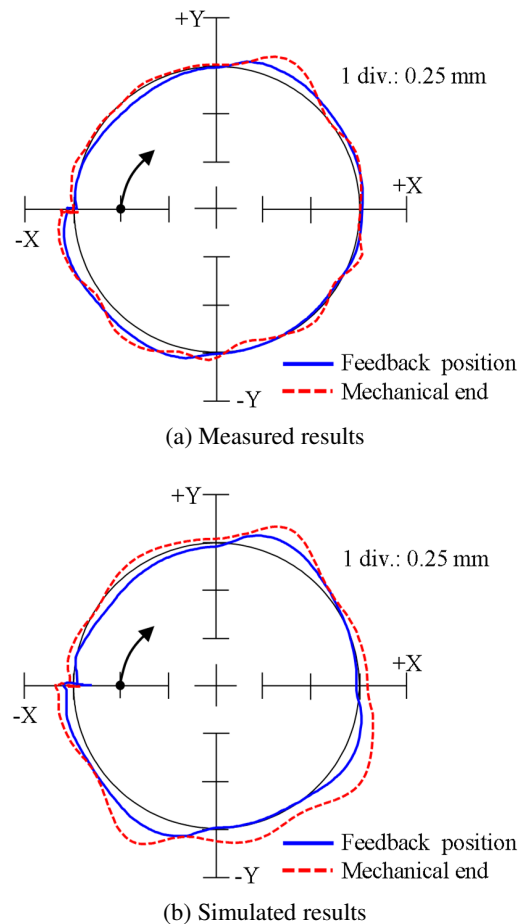


**Fig. 16.** Measured and simulated circular trajectories ( $XY$  plane, feed rate: 2000 mm/min, radius: 5 mm).

in the feedback position mainly arise from the characteristics of control systems and motors. The mechanical end trajectories show the results measured by the laser tracker. The differences between the feedback position and mechanical end represent the influence of the robot structure itself.

According to the results, a trajectory error can be observed in the first quadrant of both the measured and simulated results. Although the maximum radial errors increase in the simulated results, the shapes of the errors are similar to the measured ones.

In addition, in the third and fourth quadrants, the vibration observed on the mechanical end trajectory can also be simulated by the model. However, the simulated radial error of the mechanical end trajectory around the third and fourth quadrants is larger than the measured error. The reason for the inaccurate simulation was not clarified in this study. It is expected that the simulation accuracy of the trajectories can be improved if the frequency responses can be accurately simulated. However, although the simulated trajectory cannot perfectly match the measured trajectory, it can be concluded that the proposed model can adequately express the trend of dynamic motion errors of the robot owing to the dynamic characteristics, including the influence of joint bearing stiffness.

## 6. Conclusions

In this study, the vibration mode of an industrial architectural robot was analyzed based on the measured frequency characteristics. According to the results of the modal analysis, it was clarified that the axial and angular stiffness of the bearings of each joint of the robot significantly impacted the vibration characteristics. Therefore, a mathematical model of the robot was developed by considering the joint bearing stiffness. The mathematical model that also considered the kinematics of the robot, stiffness of reduction gears, control system for motors, and disturbances, such as friction and gravity was introduced into the model.

The validity of the model was confirmed through simulations of the vibration mode and circular trajectories. As a result, it is confirmed that the proposed model can adequately express the vibration owing to the joint bearing stiffness, except for the simulation accuracy. It is also confirmed that the proposed model can adequately express the trend of dynamic motion errors of the robot owing to its dynamic characteristics, including the influence of joint bearing stiffness.

The authors will try to improve the simulation accuracy by developing new parameter identification methods. Control techniques that can suppress vibrations will also be considered based on the model.

### Acknowledgements

The authors would like to sincerely acknowledge the contributions of Mr. Okamoto and Mr. Ohka, who were the master's and undergraduate students of Kobe University.

### References:

- [1] "Industrial Robotics – Insights into the Sector's Future Growth Dynamics," McKinsey & Company, 2019.
- [2] D. Kostic, B. Jager, and R. Hensen, "Modeling and Identification for High-Performance Robot Control: An RRR-Robotic Arm Case Study," *IEEE Trans. on Control Systems Technology*, Vol.12, No.6, pp. 904-919, 2004.
- [3] A. Verl, A. Valente, S. Melkote, C. Brecher, E. Ozturk, and L. T. Tunk, "Robots in Machining," *CIRP Annals – Manufacturing Technology*, Vol.68, pp. 799-822, 2019.
- [4] D. Milutinovic, M. Glavonjic, N. Slavkovic, Z. Dimic, S. Zivanovic, B. Kokotovic, and L. Tanovic, "Reconfigurable Robotic Machining System Controlled and Programmed in a Machine Tool Manner," *Int. J. of Advanced Manufacturing Technology*, Vol.53, pp. 1217-1229, 2011.
- [5] N. Slavkovic, D. Milutinovic, and M. Glavonjic, "A Method for Off-line Compensation of Cutting Force-induced Errors in Robotic Machining by Tool Path Modification," *Int. J. of Advanced Manufacturing Technology*, Vol.70, pp. 2083-2096, 2015.
- [6] A. Hayashi, H. Tanaka, M. Ueki, H. Yamaoka, N. Fujiki, and Y. Morimoto, "Forward Kinematics Model for Evaluation of Machining Performance of Robot Type Machine Tool," *Int. J. Automation Technol.*, Vol.15, No.2, pp. 215-223, 2021.
- [7] M. F. Zaeh and O. Roesch, "Forward Kinematics Model for Evaluation of Machining Performance of Robot Type Machine Tool," *Int. J. Automation Technol.*, Vol.9, No.2, pp. 129-133, 2015.
- [8] L. B. Silva, H. Yoshioka, H. Shinno, and J. Zhu, "Tool Orientation Angle Optimization for a Multi-Axis Robotic Milling System," *Int. J. Automation Technol.*, Vol.13, No.5, pp. 574-582, 2019.
- [9] Y. Altintas and E. Budak, "Analytical Prediction of Stability Lobes in Milling," *CIRP Annals – Manufacturing Technology*, Vol.44, pp. 357-362, 1995.
- [10] G. Quintana and J. Ciurana, "Chatter in Machining Process: a Review," *Int. J. of Machine Tools and Manufacture*, Vol.51, pp. 363-376, 2011.
- [11] H. Mayeda, "Dynamic Models of Robot Arm and Its Identification," *J. of the Robotics Society of Japan*, Vol.7, No.2, pp. 95-100, 1989 (in Japanese).
- [12] O. Zirn, "Machine Tool Analysis – Modelling, Simulation and Control of Machine Tool Manipulators," A Habilitation Thesis, ETH Zurich, 2008.
- [13] S. Cubero, "Industrial Robotics – Theory, Modelling and Control," PLV Pro Literatur Verlag Robert Mayer-Scholz, 2007.
- [14] L. Ding, H. Wu, Y. Yao, and Y. Yang, "Dynamic Model Identification for 6-DOF Industrial Robots," *J. of Robotics*, Vol.2015, Article ID 471478, 2015.
- [15] T. Yasuo, Y. Omaki, T. Nampo, and H. Mayeda, "Identification and Model Based Control of a 6 D.O.F. Industrial Manipulator," *Proc. of IFAC Robot Control*, pp. 111-117, 1997.
- [16] M. M. Olsen and H. G. Petersen, "A New Method for Estimating Parameters of a Dynamic Robot Model," *IEEE Trans. on Robotics and Automation*, Vol.17, No.1, pp. 95-100, 2001.
- [17] J. J. Craig, P. Hsu, and S. S. Sastry, "Adaptive Control of Mechanical Manipulators," *The Int. J. of Robotics Research*, Vol.6, No.2, pp. 16-28, 1987.
- [18] N. D. Vuong and M. H. Ang Jr., "Dynamic Model Identification for Industrial Robots," *Acta Polytechnica Hungarica*, Vol.6, No.5, pp. 51-68, 2009.
- [19] L. Ding, X. Li, Q. Li, and Y. Chao, "Nonlinear Friction and Dynamical Identification for a Robot Manipulator with Improved Cuckoo Search Algorithm," *J. of Robotics*, Vol.2018, Article ID 8219123, 2018.
- [20] M. C. Good, L. M. Sweet, and K. L. Strobel, "Dynamic Models for Control System Design of Integrated Robot and Drive Systems," *ASME J. of Dynamic Systems, Measurement, and Control*, Vol.107, pp. 53-59, 1985.
- [21] H. N. Huynh, G. Kouroussis, and O. Verlinden, "Modal Updating of a 6-axis Robot for Milling Application," *Proc. of the 25th Int. Congress on Sound and Vibration*, 2018.
- [22] H. N. Huynh, H. Assadi, E. Riviere-Lorpehvre, O. Verlinden, and K. Ahmadi, "Modelling the Dynamics of Industrial Robots for Milling Operations," *Robotics and Computer-Integrated Manufacturing*, Vol.61, Article 101852, 2020.
- [23] M. Bottin, S. Cocuzza, N. Comand, and A. Doria, "Modeling and Identification of an Industrial Robot with a Selective Modal Approach," *Applied Science*, Vol.10, Article 4619, 2020.
- [24] R. Sato, G. Tashiro, and K. Shirase, "Analysis of the Coupled Vibration between Feed Drive Systems and Machine Tool Structure," *Int. J. Automation Technol.*, Vol.9, No.6, pp. 689-697, 2015.
- [25] N. W. Spong, S. Hutchinson, and M. Vidyasagar, "Robot Modeling and Control," John Wiley and Sons, Inc., 2005.
- [26] R. Sato, "Feed Drive Simulator," *Int. J. Automation Technol.*, Vol.5, No.6, pp. 875-882, 2011.
- [27] J. H. Holland, "Adaptation in Natural and Artificial Systems," The University of Michigan Press, 1975.
- [28] ISO 230-4, "Test Code for Machine Tools – Part 4: Circular Tests for Numerically Controlled Machine Tools," 2005.



**Name:**  
Ryuta Sato

**Affiliation:**  
Associate Professor, Department of Mechanical Engineering, Graduate School of Engineering, Kobe University

**Address:**  
1-1 Rokko-dai, Nada, Kobe 657-8501, Japan

**Brief Biographical History:**  
2004- Research Associate, Tokyo University of Agriculture and Technology  
2008- Researcher, Mitsubishi Electric Corporation  
2010- Assistant Professor, Kobe University  
2013- Associate Professor, Kobe University

**Main Works:**

- “Analytical Time Constant Design for Jerk-limited Acceleration Profiles to Minimize Residual Vibration after Positioning Operation in NC Machine Tools,” *Precision Engineering*, Vol.71, pp. 47-56, 2021.
- “Active Contouring Control of NC Machine Tools for High Speed Contouring Motions,” *J. of Advanced Mechanical Design, Systems, and Manufacturing*, Vol.14, No.1, 19-00274, 2020.
- “Influence of Non-linear Friction Characteristics and Process Damping in Milling Operations,” *Precision Engineering*, Vol.61, pp. 103-109, 2019.

**Membership in Academic Societies:**

- Japan Society of Mechanical Engineers (JSME)
- Japan Society for Precision Engineering (JSPE)
- Society of Instrument and Control Engineers (SICE)

---



**Name:**  
Yuya Ito

**Affiliation:**  
Handling Robot Development Department, FA Robot Division, DAIHEN Corporation

**Address:**  
4-1 Koyo-cho Nishi, Higashinada-ku, Kobe 658-0033, Japan

**Brief Biographical History:**  
2013- Engineer, DAIHEN Corporation

---



**Name:**  
Shigeto Mizuura

**Affiliation:**  
General Manager, Handling Robot Development Department, FA Robot Division, DAIHEN Corporation

**Address:**  
4-1 Koyo-cho Nishi, Higashinada-ku, Kobe 658-0033, Japan

**Brief Biographical History:**  
1992- Engineer, DAIHEN Corporation  
2010- Manager, Engineering Department, DAIHEN Corporation  
2018- General Manager, DAIHEN Corporation

---



**Name:**  
Keiichi Shirase

**Affiliation:**  
Professor, Department of Mechanical Engineering, Graduate School of Engineering, Kobe University

**Address:**  
1-1 Rokko-dai, Nada, Kobe 657-8501, Japan

**Brief Biographical History:**  
1984- Research Associate, Kanazawa University  
1995- Associate Professor, Kanazawa University  
1996- Associate Professor, Osaka University  
2003- Professor, Kobe University

**Main Works:**

- K. Shirase and K. Nakamoto, “Simulation Technologies for the Development of an Autonomous and Intelligent Machine Tool,” *Int. J. Automation Technol.*, Vol.7, No.1, pp. 6-15, 2013.
- T. Kobayashi, T. Hirooka, A. Hakotani, R. Sato, and K. Shirase, “Tool Motion Control Referring to Voxel Information of Removal Volume Voxel Model to Achieve Autonomous Milling Operation,” *Int. J. Automation Technol.*, Vol.8, No.6, pp. 792-800, 2014.
- M. M. Isnaini, Y. Shinoki, R. Sato, and K. Shirase, “Development of CAD-CAM Interaction System to Generate Flexible Machining Process Plan,” *Int. J. Automation Technol.*, Vol.9, No.2, pp. 104-114, 2015.
- I. Nishida, R. Okumura, R. Sato, and K. Shirase, “Cutting Force Simulation in Minute Time Resolution for Ball End Milling Under Various Tool Posture,” *ASME J. of Manufacturing Science and Engineering*, Vol.140, No.2, doi: 10.1115/1.4037427, 2018.
- K. Kaneko, I. Nishida, R. Sato, and K. Shirase, “Machining state monitoring in end milling based on comparison of monitoring and predicted cutting torques,” *J. of Advanced Mechanical Design, Systems, and Manufacturing*, Vol.13, No.3, doi: 10.1299/jamdsm.2019jamdsm0052, 2019.
- I. Nishida, R. Tsuyama, K. Shirase, M. Onishi, and K. Koarashi, “Development of Innovative Intelligent Machine Tool based on CAM-CNC Integration Concept – Adaptive Control based on Predicted Cutting Force –,” *Int. J. Automation Technol.*, Vol.13, No.3, pp. 373-381, 2019.

**Membership in Academic Societies:**

- American Society of Mechanical Engineers (ASME)
- Society of Manufacturing Engineers (SME)
- Japan Society of Mechanical Engineers (JSME), Fellow
- Japan Society for Precision Engineering (JSPE), Fellow

---